OPEN ACCESS

Non-linear optical measurements and crystalline characterization of CdTe nanoparticles produced by the 'electropulse' technique

New Journal of Physics
An Institute of Physics and Deutsche Physikalische Gesellschaft Journal

Non-linear optical measurements and crystalline characterization of CdTe nanoparticles produced by the 'electropulse' technique

Jerome Loicq[1], **Yvon Renotte**[1], **Jean-Luc Delplancke**[2] **and Yves Lion**[1]

[1] Hololab, Institute of Physics, Bat B5a, University of Liege, 4000 Liege, Belgium
[2] Science des Matériaux et Electrochimie, CP194/03, Université Libre de Bruxelles, B1050 Bruxelles, Belgium
E-mail: J.loicq@ulg.ac.be

New Journal of Physics **6** (2004) 32
Received 9 December 2003
Published 15 March 2004
Online at http://www.njp.org/ (DOI: 10.1088/1367-2630/6/1/032)

Abstract. We propose to extend the 'electropulse' technique to synthesize CdTe nanoparticles for optical components. To do so, we create nuclei of the expected material on a titanium electrode immersed in an electrolytic solution by using an electrochemical pulse. The nanoparticles are expelled from the titanium horn surface by cavitation bubbles, which are produced in the solution by a high intensity ultrasound pulse generated by a piezoelectric crystal. Optical absorption spectra and third-order non-linear optical properties of a colloidal solution of CdTe particles produced by this technique are presented. The non-linear refractive index was characterized using the single-beam z-scan technique, and measurements were carried out at several incidence intensities. Non-linear indices of refraction between -1.2×10^{-7} and -2×10^{-8} cm^2 W^{-1} were measured.

PII: S1367-2630(04)73155-9

Contents

1. Introduction

Non-linear optics is considered to be a new frontier area between science and technology. It is expected to play an essential role in the emergent technology of photonics. Recently, molecular materials, polymeric systems and nanocrystals have emerged as a new range of promising materials for achieving optimization of non-linear optical properties and their applications in new devices.

Synthesis of materials of nanometric dimensions has rapidly expanded in the last few years. Structures with a controlled size and shape, from clusters with a few atoms to nanostructures with some thousands of atoms, can be produced with a predefinite architecture. At the nanometric scale, materials possess special chemical and physical properties which are modified by quantum confinement of the electrons. These properties strongly depend on the shape and size of the particles and they differ from those in the macroscopic scale.

Interaction of II–VI semiconductor materials with light has been studied. Nanoparticles present some strong electronic resonance effects near which non-linear optical properties were observed [1]–[4]. Electronic and optical properties of nanocrystalline semiconductors are specific because of the quantum confinement defined as the elementary electronic excitation in a reduced volume. This is a step between the bulk and an atom. Quantum confinement acts especially on quasiparticle excitons [5, 6]. Such materials are very promising for optoelectronic design. The 'electropulse' technique is a technique to produce semiconductor nanoparticles. The non-linear optical properties of CdTe colloidal solutions are analysed by the single beam z-scan technique, which is based on the intensity-dependent refractive index. The overall refractive index of the material is given by $n = n_o + n_2 I$, where n_2 is called the non-linear refractive index. It originates from the third-order susceptibility of the material, which cannot be neglected when the incident light intensity is high.

2. Synthesis of CdTe nanoparticles

Different methods have been developed for the synthesis of semiconductor nanoparticles. Among these one can cite nanocrystallite growth '*in situ*' inside porous glass matrix with a controlled pore size, prepared by the sol–gel technique [7, 8], growth in an ionic crystal [9], or growth in a zeolite [10]. Several researchers have explored the two most popular methods of synthesis of the II–VI semiconductors developed by Murray *et al* [11] and the aqueous

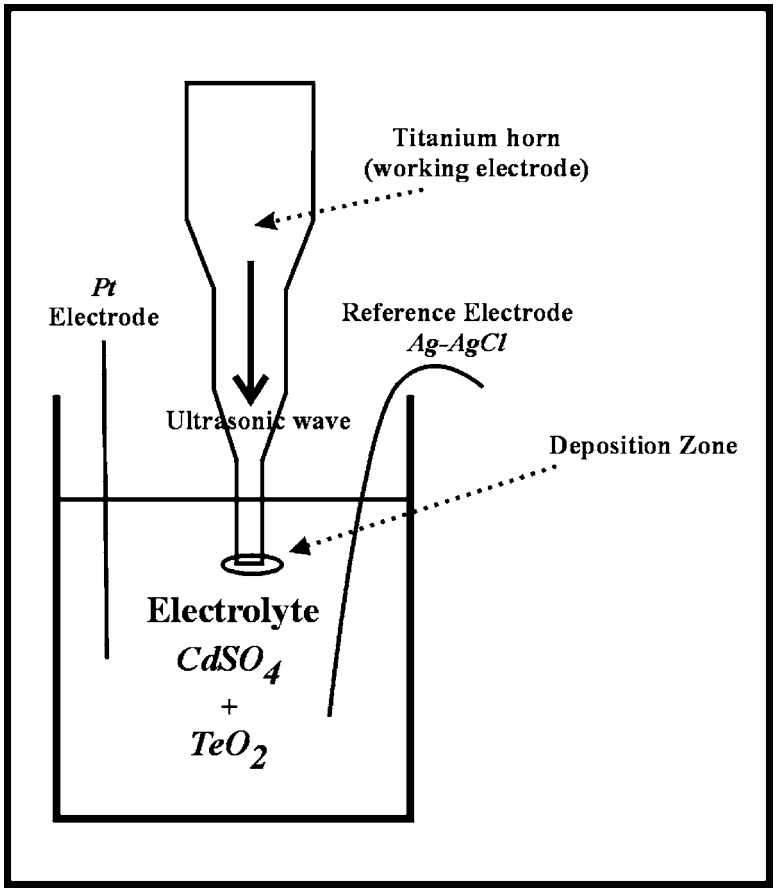

Figure 1. 'Electropulse' technique: experimental setup.

preparation technique pioneered by Henglein and Weller [12, 13]. The 'electropulse' technique is derived from electrochemistry. The experimental setup was developed at the Université Libre de Bruxelles (ULB), by Delplancke's group [14]–[17]. An electrochemical growth process is divided into three steps: a random germ nucleation on the working electrode's surface, their independent growth under the continuous influence of electric field and current and, finally, the total surface coverage with the deposited compound. The production of nanocrystals results only from the first two steps. Next, the nanoparticles are expelled out of the titanium horn by the cavitation bubble produced by an intense ultrasound field.

High-intensity ultrasound waves were produced in the titanium horn combined with two piezoelectric ceramic elements. These were placed between a counter mass and the titanium rod and connected to a high-frequency alternative generator. The resonance frequency of the titanium horn and the ultrasonic frequency produced inside the horn have a value of around 20 kHz. The intensity of the ultrasound wave was typically 50 W cm^{-2} on the small area where the deposition occurred (cf figure 1). The experimental conditions were adjusted to be above the cavitation threshold of the electrolyte solution. Under ultrasound irradiation, a cloud of bubbles appeared below the titanium horn. The implosion of these bubbles propelled a jet of liquid perpendicular to the substrate. This jet was able to detach the previously electrochemically synthesized particles from the titanium horn surface. A sequential mode was used. T_{on} is the deposition interval time and controls the nanoparticles' size, T_{off} the non-deposition time and

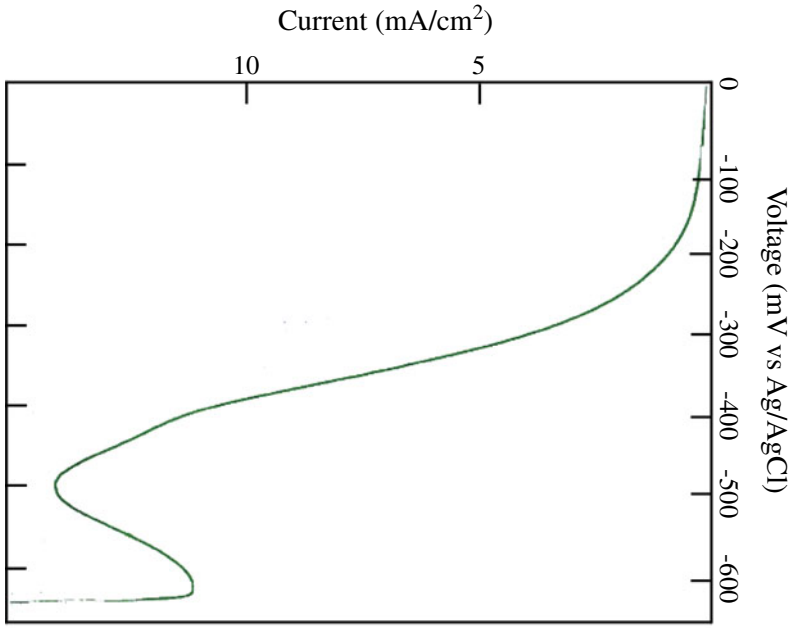

Figure 2. Experimental polarization curve of the titanium substrate in the Cd/Te electrolyte.

T_{us} the ultrasound duration time. The size of the particles was directly linked to the times T_{on} (in the hundreds of milliseconds range). The titanium horn was connected to a Tacussel PRT-20X potentiostat. The electrochemical design was a three-electrode configuration. The titanium electrode was named as the 'working electrode', on which the deposition occurs. The reference electrode was an Ag/AgCl electrode and the anode (or counterelectrode) was a platinum foil.

Results from previous studies [18] dictated the choice of the electrolyte: $CdSO_4$ (1M), $HTeO_2^+$ (40–150 μM) solution obtained with the form of TeO_2 in aqueous solution at pH = 2.4 adjusted by sulphuric acid (H_2SO_4). The temperature of the solution was maintained at 85 °C. The measurement of the polarization curve of the titanium substrate in the electrolyte used is illustrated in figure 2. Deposition takes place between −200 and −600 mV with reference to the Ag/AgCl electrode. The optimum value of the potential for the production of the stoichiometric CdTe compound was determined by long constant-potential deposition experiments. X-ray diffraction analysis of the deposits obtained was then performed. This value was −570 mV referring to the Ag/AgCl reference electrode and the 'working electrode'. The electrochemical process is potentiostatic, which means that the potential is controlled and the current intensity across the solution is automatically determined by the nature of the electrolyte, shown in figure 2.

This technique allows us to produce CdTe nanoparticles with a mean radius ranging between 4 and 200 nm, which correspond to deposition times, T_{on} of 5 and 400 ms respectively. The preliminary preparation of the 'working electrode' is a rather important step to produce particles of good quality. This electrode must be carefully polished (roughness must be less than 30 μm). Next, a thin film of TiO_2 is coated on the deposition zone of the working electrode. This film favours the instantaneous nucleation and growth process, as described in [19].

To produce an optically transparent sample, optical diffusion and diffraction inside the material by the aggregates of particles must be minimized. Consequently, the coalescence of

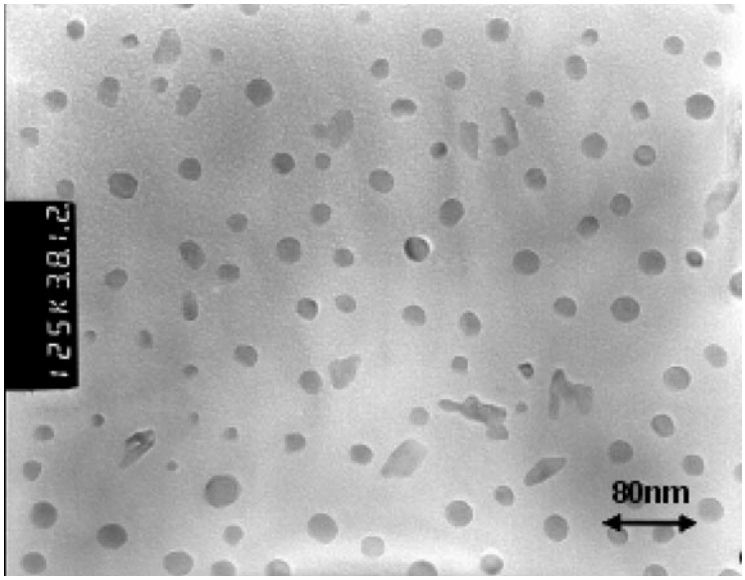

Figure 3. Imaging at 1.25×10^3 magnification of a set of CdTe particles.

quantum dots must be avoided. Moreover, the optical quality of the surface should be as soft as possible. This means that surface states resulting from defects should be annihilated, e.g. by a surfactant. Trioctyl phosphine oxide (TOPO) was used. Under these conditions, properties of the material may be linked up with an individual particle set.

Since the nanoparticles are produced in an aqueous medium, their surface is surrounded by adsorbed water molecules. The newly produced particles are filtered, dried and added to a TOPO/TOP solution at 70 °C. High intensity ultrasound waves are required to disperse the particles and to split up the aggregates. The TOPO/TOP solution with the particles is then heated to 230 °C for half an hour under continuous magnetic stirring. Before adding methanol in excess to precipitate the particles, the temperature is reduced to 60 °C. Finally, the TOPO coated particles are dispersed in a non-polar solvent such as toluene or hexane. The colloidal solution remains stable for several weeks.

3. Crystalline characterization of nanocrystals

The nanocrystals were characterized by high-resolution scanning transmission electron microscopy (STEM), x-ray fluorescence (XRF) and x-ray diffraction (XRD). Figure 3 is a 125×10^3 times magnified image of a set of CdTe particles with low crystallite coverage on the copper grid. It allows statistic size measurement of ∼100 individual nanocrystallites on the image. The average size is 22 nm ± 10%. Moreover, it shows that particles are not agglomerates.

Figure 4 is a blow-up of figure 3. The selected particle has a size of 22 nm and is of spherical symmetry. This is an interesting result since, due to the growth of the particle on a plane, it was expected to grow along the axis perpendicular to the plane of the horn. In the nanometre scale, the sizes of the nuclei were so small that the surface-free-energy minimum corresponds to a pseudo-spherical symmetry. Figure 5 illustrates the size distribution of the particles present in figure 3. Figure 6 depicts a very high magnification, 1.15×10^6 times, of a single particle. Attention is focused on one particle pulled out of a sample of quantum dots with a mean radius

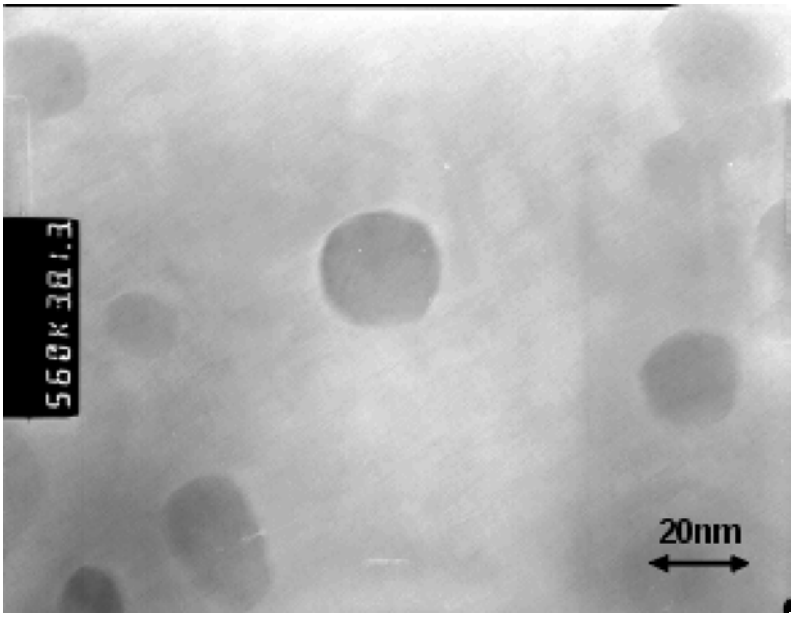

Figure 4. Imaging at blow-up of figure 3.

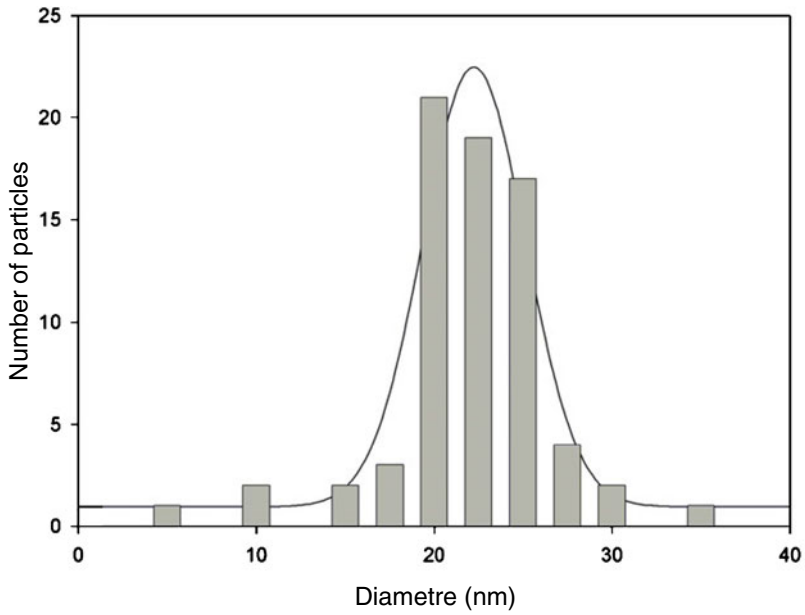

Figure 5. Size distribution of the sample presented in figure 3.

of 6 nm $\pm$ 7%. Despite the pseudo-spherical symmetry, cleavage planes are easy to identify in figure 6. The statistical measurements were repeated for the different samples presented in this paper. The distribution width varies from 7 to 10%. Table 1 shows the different samples synthesized in this work. The distribution width is explained by a more or less deep alteration of the deposition surface and of the TiO_2 film. Moreover, during pulse sequences, ultrasound waves are not always evenly distributed on the horn surface. The difference in surface-polishing from one experiment to another and the accumulation of material attached to the horn are two

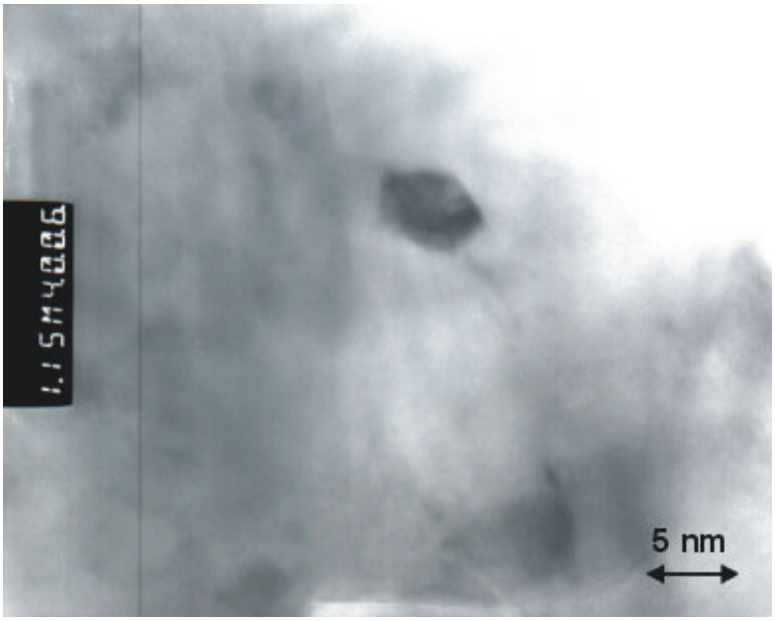

Figure 6. Imaging at 1.15×10^6 times magnification of a single particle.

Table 1. Parameters of the samples.

	Deposition time (ms)	Particle size (nm)	Size dispersion (%)	Optical density (633 nm)
a	200	100	±7	0.06
b	50	30	±7	0.05
c	20	22	±10	0.21
d	10	12	±8	0.22
e	5	4	±7.5	0.17

probable reasons for the lack of homogeneity of the ultrasound pulses. They indeed locally modify the resonance frequency of the horn. Nevertheless, the dispersion in the size distribution can be improved by selective precipitation after synthesis.

X-ray diffraction (XRD) and EDX are useful to determine the crystalline character and the composition of the samples. Figure 7 illustrates the results of XRD; the structure of nanoparticles is periodical, crystalline and corresponds to the cubic structure of CdTe. All samples showed similar diffraction spectra. The widening of the peaks, due to the Sherrer effect, is an argument in favour of the small sizes of the particles, confirmed by electron microscope results. However, figure 7 shows the presence of TeO_2 but in very small amounts. It comes from non-dissolved Te reactant (TeO_2) in the aqueous solution. EDX measures the atomic composition of the nanoparticles: Cd and Te are found in equal amounts in all samples.

4. Linear optical absorption spectra of nanocrystals

It is known that decreasing the size of nanometric particles induces a blue shift in the energy gap and a set of discrete energy levels in the semiconductor. This is the effect of quantum

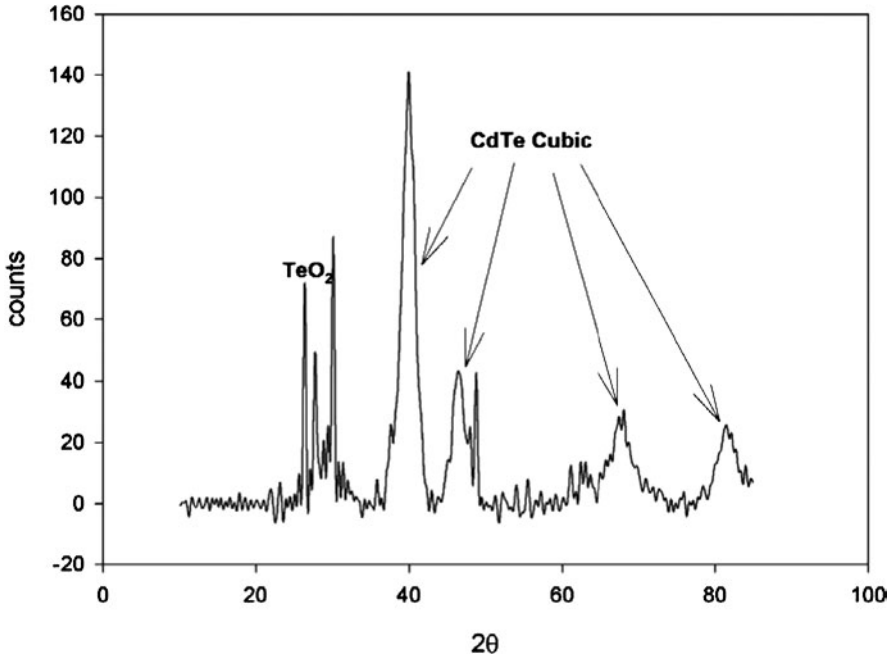

Figure 7. Diffraction diagram of the sample e: CdTe cubic structure is detected. Residual TeO_2 is also present.

confinement, which occurs mainly on the exciton quasi-particle energy levels. The spectrum (figures 8 and 9) has been recorded on a low-concentration colloidal solution of CdTe in toluene solution. The recording temperature was 300 K and the scan rate was 120 nm min^{-1} with a resolution of 1 nm. The spectrophotometer was a PerkinElmer 559 UV/Vis. Absorption spectra show the evolution of the energy levels' distribution with the particle sizes. Two spectra are shown in figure 8. The first spectrum (continuous line) corresponds to a several minute duration deposition under the deposition conditions described previously. It produces particles bigger than 1 μm. The larger particles are characterized by an absorption spectrum similar to the one shown by bulk CdTe. The dashed line is the absorption spectrum of 100 nm particles. In figure 9 are gathered the absorption spectra of the particles b–e from table 1. The blue shift corresponding to the evolution of the first excited state absorption towards the short wavelengths is noticeable. This state corresponds to the creation of an exciton, the binding state of an electron and a hole. The peaks of the spectrum of sample c are not clear, and the large size distribution is responsible for the widening of the absorption peaks. Table 1 shows also the optical density of the nanoparticles at 633 nm which is the excitation wavelength of the z-scan setup. Rayleigh scattering was subtracted from the curves to obtain the response of purely the nanoparticles.

5. Non-linear optics: z-scan

The z-scan technique is used to characterize the non-linear optical properties of CdTe colloidal solutions. Developed by Sheik-Bahae *et al* [20], the z-scan allows the characterization of transparent materials having third-order non-linear effects. It is based on the intensity-dependent refractive index and includes the variation of the refractive index as a function of the incident

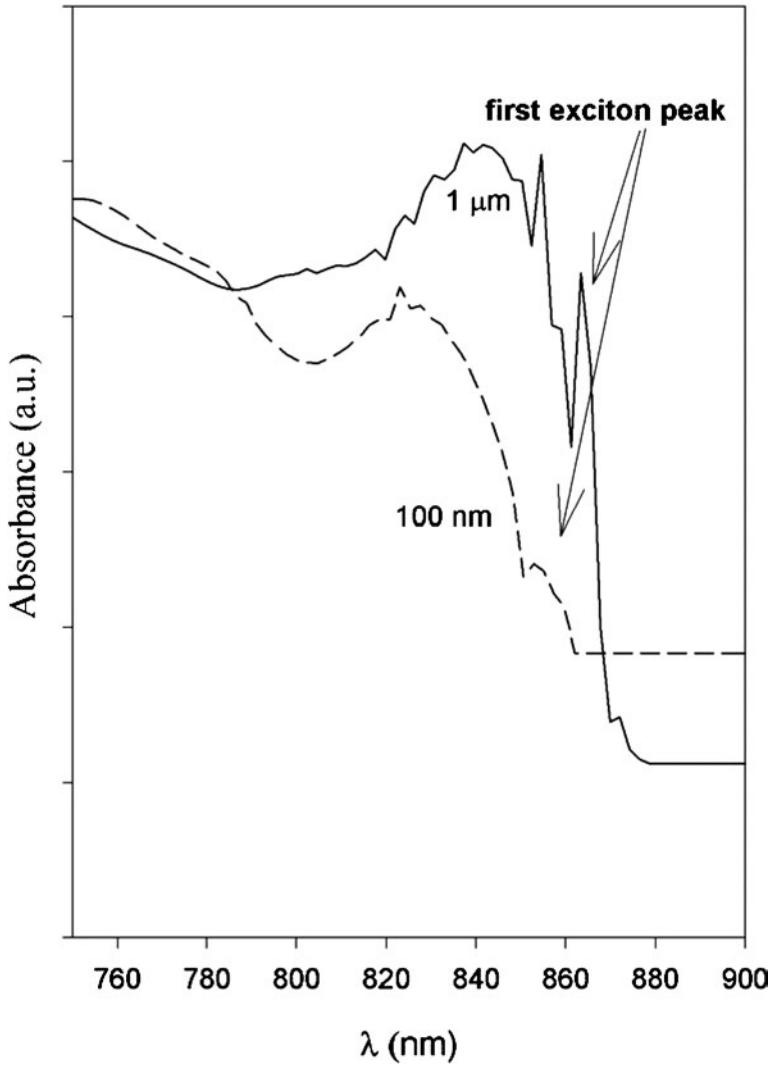

Figure 8. Absorption spectra of 1 μm (continuous line) and 100 nm (dashed line) CdTe particle.

beam irradiance on the sample:

$$n = n_o + n_2 I, \tag{1}$$

where n is the index of refraction, n_o the linear index, I the intensity and n_2 the non-linear index of refraction. It is associated with the real part of $\chi^{(3)}$ in the Taylor expansion of the material's polarizability.

A Gaussian radial distribution of the incident laser beam (T_{00} mode) induces a refractive index modulation inside the sample. Consequently, this modulation involves the creation of an induced lens. The z-scan is therefore an auto-induced technique.

The principle is to move the sample along the optical axis in the vicinity of the laser beam focused on an external lens. For each position of the sample around the focus, the induced lens inside the sample possesses different focal lengths. This focal length depends on the incident Gaussian shape. The experiment consists of the measurement of the irradiance

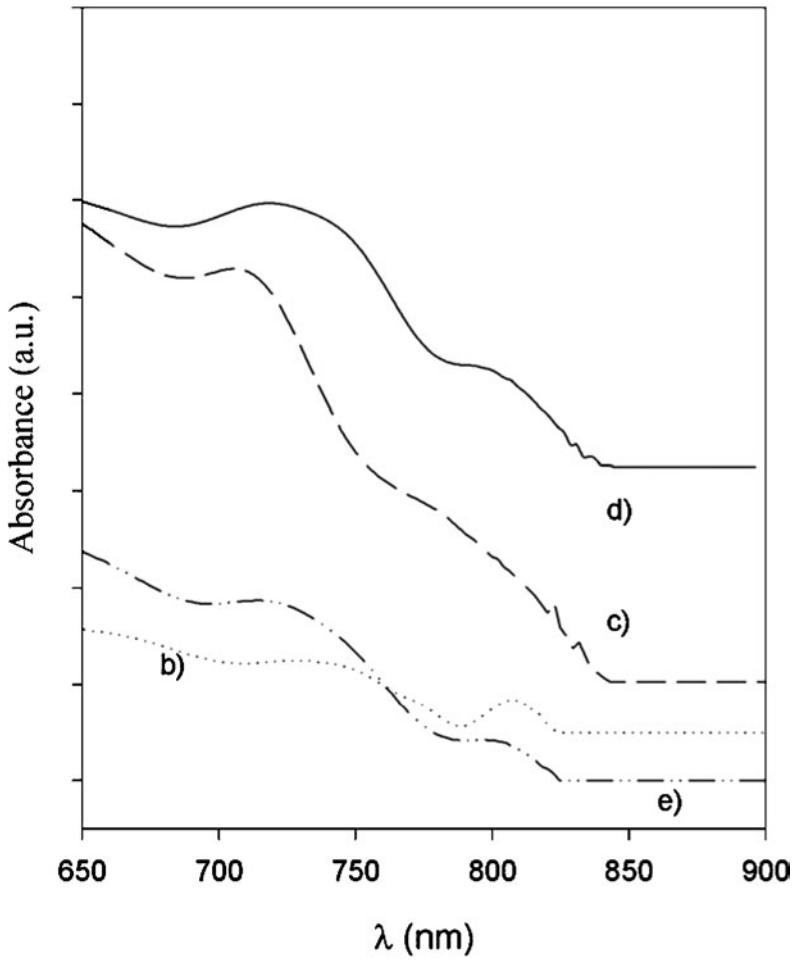

Figure 9. Set of absoption spectra for the samples in table 1.

through a small aperture in a far field for each position versus the focus position. The sign of n_2 determines the vergence of the lens, positive or negative. For a positive n_2 (convergent lens), and a negative sample position (versus the external lens focus), the transmitted beam is radially wider at the aperture compared with the beam without sample because the beam converges before the focus of the fixed lens and hence the transmitted irradiance through the aperture is then lower. Consequently, for a sample position between the focus and the aperture (positive z) the focalization due to the induced lens in the sample occurs after the focus of the fixed lens and hence the irradiance at the aperture increases. A similar reasoning can be made for a divergent induced lens. The result is then the opposite.

The experimental setup is shown in figure 10. The laser is a 20 mW He–Ne continuous laser. Parameters were carefully determined by a beam analyser (Beamscan 1180 from Photon Inc.). The beam waist ($\omega_o = 63\,\mu$m) and the Rayleigh length ($z_o = 17.5$ mm) are determined. The sample is a 1 mm thick quartz cell filled with CdTe colloidal solution, see table 1. The weight fraction of CdTe crystallites in each sample is about 10%. As the sample did not present any non-linear absorption, the curve fitting is computed by the following empirical law:

$$T(z) = 1 + \frac{4\Delta\Phi_o(z/z_o)}{(1 + (z/z_o)^2)(9 + (z/z_o)^2)} \tag{2}$$

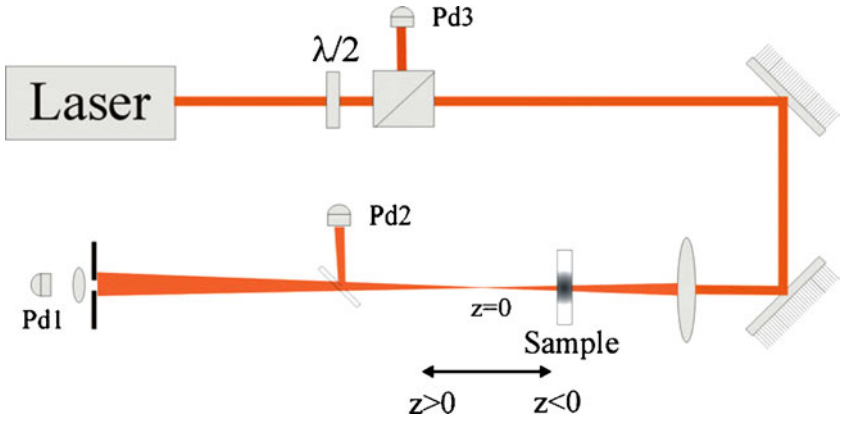

Figure 10. Z-scan experimental setup.

with

$$\Delta\Phi_o = \frac{2\pi}{\lambda} n_2 I_o L_{eff}, \tag{3}$$

where n_2 is the non-linear index of refraction from equation (1), λ the wavelength, I_o the on-axis intensity at the waist and $L_{eff} = (1 - e^{-\alpha L})/\alpha$.

$$\mathrm{Re}(\chi^{(3)})(\mathrm{cm}^2/\mathrm{W}) = \frac{n_o n_2(\mathrm{cm}^2/\mathrm{W})}{3\pi}. \tag{4}$$

The analysed samples are those described in table 1. The data were collected for different incident beam intensities. The half-wave plate shown in the setup of figure 10 allows an efficient and simple tuning of the beam intensity. The output laser intensities were 0.5, 1, 2, 3, 4, 5 mW respectively. Figure 11 illustrates the results obtained for sample c. As expected, the non-linear features increase when the beam intensity increases. This is due to the fact that the weight of the second term of the equation describing the intensity-dependent refractive index increases.

Equation (2) is valid until $|\Delta\Phi_o|$ value is less than π [4]. It gives a relative uncertainty on $|\Delta\Phi_o|$ of 3%. The error propagation calculation gives an n_2 value of approximately 9% for each measure. The principal error sources come from intensity and waist measurements. It is indicated by the error bars in figure 12.

Figure 12 shows the variation of the non-linear refractive index versus the incident beam intensity for samples b–e. The phase modulation associated with the intensity-dependent refractive index as well as the Gaussian profile of the beam decreases for all samples when the intensities are high. However, for the smaller size samples (d and e), the onset of the curve is different. The local warming, which produces a circular temperature gradient, creates a local variation of the refractive index called a thermal lens. Reference [21] reports cw non-linear optical measurement on CdTe nanoparticles embedded in a glass matrix. The non-linear refractive index value reported is of the order of 10^{-7} esu (i.e. around 10^{-9} cm^2 W^{-1}). In our measurements the n_2 values reported are greater. The explanation arises from the thermal conductivity of the surrounding nanoparticles. The thermal lens created is more pronounced as the thermal conductivity is weak. It is the case in our measurements. Thermal conductivity of glass is 1.38 W m^{-1} K^{-1} at 20 °C and increases with temperature whereas the thermal conductivity of toluene is 0.120 W m^{-1} K^{-1} and decreases with temperature [22]. Obviously, it has been

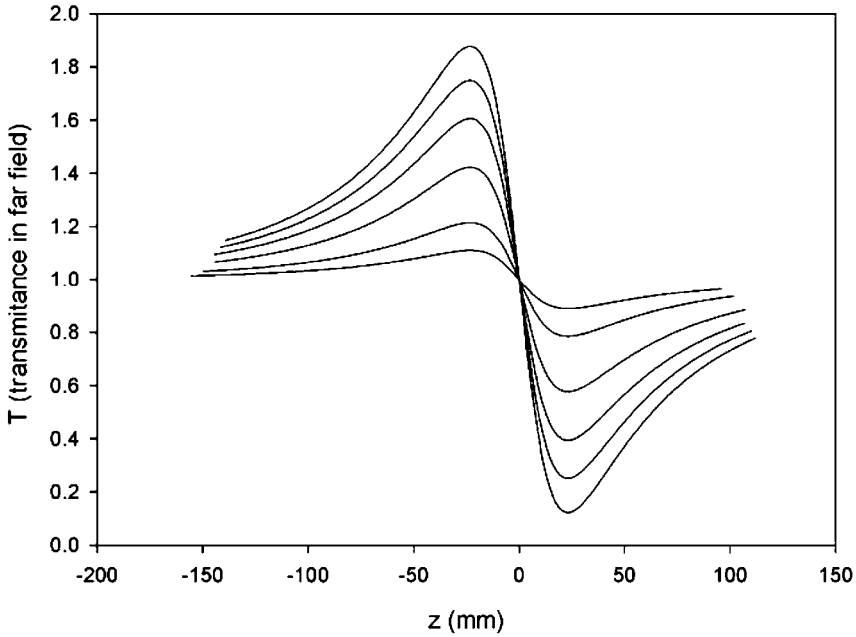

Figure 11. Z-scan curves of the sample e for different values of the incident intensity.

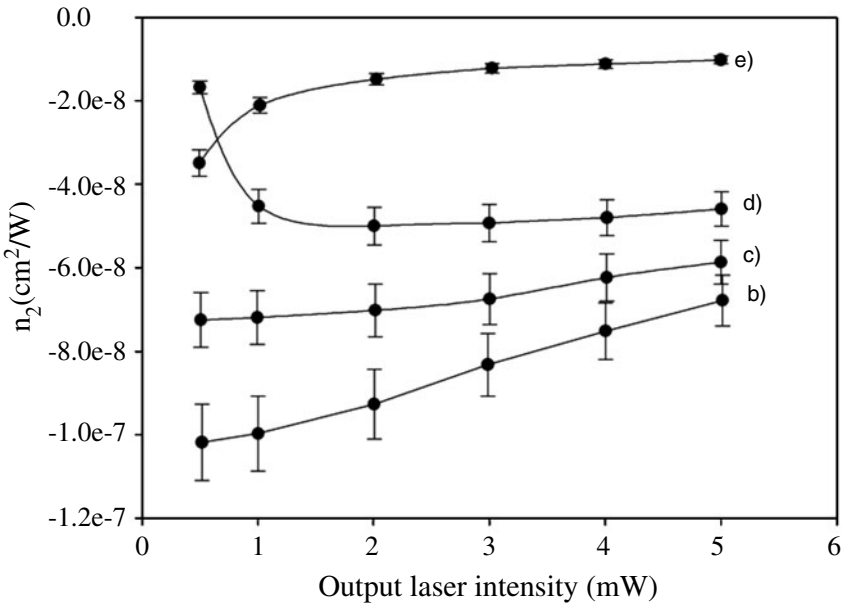

Figure 12. Comparisons of n_2 values for all samples from table 1.

verified that, under these conditions, the solvent alone did not show any non-linear effect. No non-linear absorption was detected at the He–Ne laser emission wavelength.

Non-linear optical measurement with a pulsed laser has been reported in [23, 24]. These measurements are very different from the measurements presented in this paper. In [23, 24], electronic effects contributed to the intensity-dependent refractive index whereas in the present measurements it is due to thermal effects.

6. Conclusion

CdTe nanoparticles were synthesized by the 'electropulse technique'. X-ray diffraction and EDX showed that the nanoparticles' composition corresponds to the expected CdTe percentages and that they are crystalline. Spectra recorded by HRSTEM showed that the size of the nanoparticles is nanometric, the size distribution being relatively narrow, between 7 and 10%. The exciton state of the particles is observed as a function of particle size by optical absorption measurements. Third-order optical non-linearities of a colloidal solution of CdTe in toluene were measured by the z-scan technique at the emission wavelength of a continuous wave He–Ne laser. The value of n_2 varies between -1.2×10^{-7} and $-2 \times 10^{-8}\,\mathrm{cm^2\,W^{-1}}$.

Acknowledgments

The authors would like to thank Vanessa Rosso for her help with the z-scan measurements and Jean Dille for his help with the HRSTEM measurements.

References

[1] Garmire E and Kost A 1999 *Nonlinear Optics in Semiconductors* II (New York: Academic)
[2] Harper P and Wherrett B 1977 *Nonlinear Optics* (New York: Academic)
[3] Saleh B E A and Teich M C 1991 *Fundamentals of Photonics* (New York: Wiley)
[4] Sutherland R 1996 *Handbook of Nonlinear Optics* (New York: Dekker)
[5] Nalwa H 2000 *Handbook of Nanostructured Materials and Nanotechnology: Optical Properties* (New York: Academic)
[6] Gaponenko S 1998 *Optical Properties of Semiconductor Nanocrystals* (Cambridge: Cambrige University Press)
[7] Cerqua K, Hayden J and Lacourse W 1998 *J. Non-Cryst. Solids* **100** 471
[8] Othmani A, Plenet J, Bernstein E, Bovier C, Dumas J, Riblet P, Grum J and Levy P G R 1994 *J. Crystal Growth* **144** 141
[9] Froehlich D, Haselhoff M, Rieman K and Itoh T 1995 *Solid State Commun.* **94** 189
[10] Wang Y and Herron N 1991 *J. Chem. Phys.* **91** 525
[11] Murray C, Norris D and Bawendi M 1993 *J. Am. Chem. Soc.* **115** 8706
[12] Henglein A 1989 *Chem. Rev.* **89** 1861
[13] Weller H, Schimdt H, Koch U, Fojtik A, Baral S, Henglein A, Kunath W and Weiss K 1986 *Chem. Phys. Lett.* **124** 557
[14] Delplancke J, Bella V D, Reisse J and Winand R 1995 *Mater. Res. Soc. Symp. Proc.* **372** 75
[15] Reisse J, Caulier T, Deckerkheer C, Fabre O, Vandercammen J, Delplancke J and Winand R 1996 *Ultrasonics Sonochem.* **3** 174
[16] Delplancke J, Bouesnard O, Reisse J and Winand R 1995 *Mater. Res. Soc. Symp. Proc.* **451** 383
[17] Durant A, Delplancke J, Reisse J and Winand R 1995 *Tetrahedron Lett.* **36** 4257
[18] Rakhshani A 1997 *J. Appl. Phys.* **81** 7988
[19] Delplancke J, Garmier A, Massiani Y and Winand R 1994 *Electrochim. Acta* **39** 1281
[20] Sheik-Bahae M, Said A, Wei E V S T H and Hagan D J 1990 *IEEE J. Quant. Electron.* **26** 760
[21] Ohtsuka S, Koyama T, Tsunetomo K, Nagata H and Tapaka S 1992 *Appl. Phys. Lett.* **61** 2953
[22] Perkins R A, Ramires M L V and Nieto de Castro C A 2000 *J. Res. Natl. Inst. Stand. Technol.* **105** 255
[23] Loicq J, Torenti C, Renotte Y, Calberg C, Delplancke J and Lion Y 2000 *Optics in Computing 2000 SPIE* **4089** 815
[24] Yu B, Zhu C and Gan F 2000 *J. Appl. Phys.* **87** 1759